RESEARCH ARTICLE

Magma mingling during the 1959 eruption of Kīlauea Iki, Hawaiʻi

Jennifer Marsh[1,2] · Marie Edmonds[1] · Bruce Houghton[3] · Iris Buisman[1] · Richard Herd[4]

Abstract

Magma mingling and mixing are common processes at basaltic volcanoes and play a fundamental role in magma petrogenesis and eruption dynamics. Mingling occurs most commonly when hot primitive magma is introduced into cooler magma. Here, we investigate a scenario whereby cool, partially degassed lava is drained back into a conduit, where it mingles with hotter, less degassed magma. The 1959 eruption of Kīlauea Iki, Hawaiʻi involved 16 high fountaining episodes. During each episode, fountains fed a lava lake in a pit crater, which then partially drained back into the conduit during and after each episode. We infer highly crystalline tachylite inclusions and streaks in the erupted crystal-poor scoria to be the result of the recycling of this drain-back lava. The crystal phases present are dendrites of plagioclase, augite and magnetite/ilmenite, at sizes of up to 10 μm. Host sideromelane glass contains 7–8 wt% MgO and the tachylite glass (up to 0.5% by area) contains 2.5–6 wt% MgO. The vesicle population in the tachylite is depleted in the smallest size classes (< 0.5 mm) and has overall lower vesicle number densities and a higher degree of vesicle coalescence than the sideromelane component. The tachylite exhibits increasingly complex 'stretching and folding' mingling textures through the episodes, with discrete blocky tachylite inclusions in episodes 1 and 3 giving way to complex, folded, thin filaments of tachylite in pyroclasts erupted in episodes 15 and 16. We calculate that a lava lake crust 8–35 cm thick may have formed in the repose times between episodes, and then foundered and been entrained into the conduit during drain-back. The recycled fragments of crust would have been reheated in the conduit, inducing glass devitrification and crystallisation of pyroxene, magnetite and plagioclase dendrites and eventually undergoing ductile flow as the temperature of the fragments approached the host magma temperature. We use simple models of magma mingling to establish that stretching and folding of recycled, ductile lava could involve thinning of the clasts by up to a factor of 10 during the timescale of the eruption, consistent with observations of streaks and filaments of tachylite erupted during episodes 15 and 16, which may have undergone multiple cycles of eruption, drain-back and reheating.

Keywords Tachylite · Magma mingling · Basalt · Lava lake · Vesiculation · Cooling

✉ Marie Edmonds
  marie.edmonds@esc.cam.ac.uk

1 Centre for the Modelling of Earthquakes and Tectonics (COMET), Department of Earth Sciences, University of Cambridge, Downing Street, Cambridge CB2 3EQ, UK

2 Earth Sciences Department, Imperial College, London, UK

3 Department of Earth Sciences, University of Hawaii, Honolulu, HI 96822, USA

4 School of Environmental Sciences, University of East Anglia, Norwich NR4 7TJ, UK

Introduction

Magma mixing and mingling are ubiquitous processes in magmatic systems (Lynn et al. 2017; Murphy et al. 1998; Neave et al. 2013; Perugini et al. 2003; Plail et al. 2018; Ruprecht et al. 2008; Schleicher et al. 2016; Sides et al. 2014a; Sparks and Marshall 1986; Sparks et al. 1977; Viccaro et al. 2006; Woods and Cowan 2009). The widely accepted definition of mingling is the physical interaction between two magma types, which results in compositional heterogeneities (Bateman 1995; Perugini and Poli 2012; Sparks and Marshall 1986)). Mingling is distinct from magma mixing, the latter of which involves chemical diffusion and the production of a homogeneous magma of intermediate composition from two or more end members (Jarvis et al. 2021). The extent to which magmas can mix, rather

than mingle, is controlled by the contrasts in their rheological properties, such as viscosity and density (Sparks and Marshall 1986). Mingling may give rise to streaks and banding or sharply-bounded inclusions or enclaves (Andrews and Manga 2014; Sparks and Marshall 1986) in volcanic and plutonic rocks. The textures of some mingled lavas have been simulated successfully using models of 'stretching and folding', whereby mingling textures are preserved up to the point at which chemical diffusion is able to homogenise the increasingly smaller heterogeneities present in the magma (Perugini et al. 2002, 2003). In many cases of magma mingling a hot, more primitive magma is inferred to have intruded a more silicic, cooler one, in a reservoir or conduit. In this contribution, however, we focus on a contrasting case: here we document the mingling of cooler into hotter magma facilitated by lava drain-back during an eruption of Kīlauea Volcano, Hawai'i.

Basaltic pyroclasts may contain sideromelane (brown, translucent glass) and occasionally, tachylite (microlite-rich and dark in colour) (Deardorff and Cashman 2017; Heiken 1978). Sideromelane and tachylite are often found together, in a single deposit, or even within a single clast. Tachylite has been found in erupted products from a large number of volcanoes: Etna (Andronico et al. 2009; Pompilio et al. 2017; Taddeucci et al. 2004), Stromboli (Lautze and Houghton 2005) and Vesuvius (Italy) (D'Oriano et al. 2011), Yasur, Vanuatu (Kremers et al. 2012), Katla, Iceland (Owen et al. 2019), Cinder Cone, California (Heiken 1978) and Parícutin, Mexico (Pioli et al. 2008). The origin of this texture is not well understood yet has significant implications for the interpretation of eruption dynamics. Tachylite has previously been interpreted as arising from extensive degassing-induced crystallisation of sluggish magma either along conduit margins (Cimarelli et al. 2010; Lautze and Houghton 2007; Taddeucci et al. 2004) or in shallow storage areas (Pioli et al. 2008); or the reheating and devitrification of recycled clasts (Burkhard 2001; D'Oriano et al. 2014; Deardorff and Cashman 2017).

Here we examine basaltic pyroclasts from the 1959 eruption of Kīlauea Iki, Hawai'i, for evidence of magma mingling related to the process of lava drain-back into the source vent. The Kīlauea Iki eruption, famous for the highest recorded episodes of lava fountaining at Kilauea, occurred on the side wall of a pit crater just outside the eastern rim of Kīlauea's summit caldera (Fig. 1). The eruption began on 14 November 1959 and lasted until 20 December 1959 and comprised a sequence of 16 closely spaced, moderate to high fountaining episodes (Eaton et al. 1987; Richter et al. 1970; Stovall et al. 2012, 2011; Wright 1973). The high fountaining produced a prominent, proximal 50-m high scoria cone, as well as a distal tephra blanket that can be mapped at least 4 km to the southwest (Fig. 1b). Owing to the eruption in a confined pit crater, much of the ejecta fell into a fountain-fed lava lake during each episode, which proceeded to drain partially back into the conduit, at the end of each episode (Eaton et al. 1987; Richter et al. 1970; Sides et al. 2014a; Stovall et al. 2012, 2011; Wallace and Anderson 1998). Each episode of fountaining was documented in detail, with observations such as fountain height, lava lake level and the timing of drain-back being recorded (Richter et al. 1970). Measurements of ground tilt during the eruptions, one of the first such records at any volcano, allowed the generation of a model of the magma budget, which provides estimates of magma supply rate from depth, as well as lava volume erupted, and drain-back lava volume (Eaton et al. 1987) (Fig. 2).
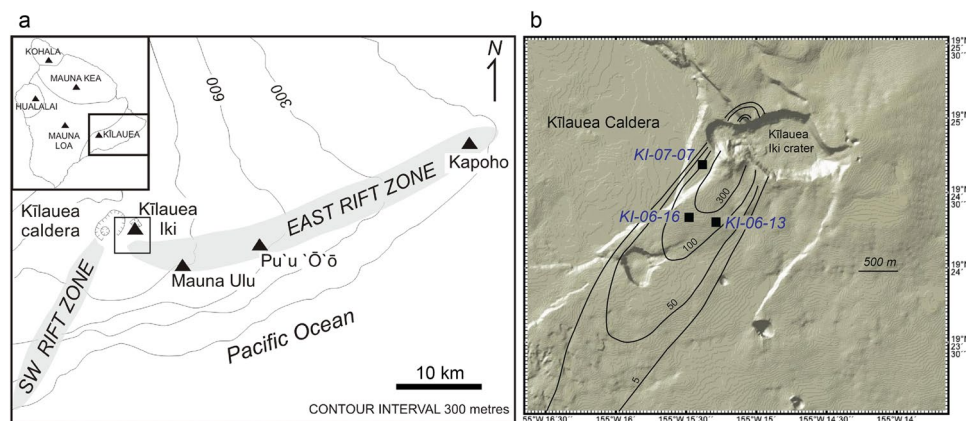

Fig. 1 Map to show the location of Kīlauea Iki, Hawai'i, and the sampling sites (Sides et al. 2014b; Stovall 2009). **a** Map to show the location of Kīlauea Iki crater and the 1959 vent on the eastern edge of the summit caldera. Kīlauea Volcano is located on the southern flank of the larger Mauna Loa volcano on the island of Hawai'i. **b** Shaded relief map to show the locations of the sampling sites KI-07–07, KI-06–16 and KI-06–13. Isopachs for the downwind tephra blanket arising from the 1959 eruption are shown, with tephra thickness in cm (Stovall 2009)
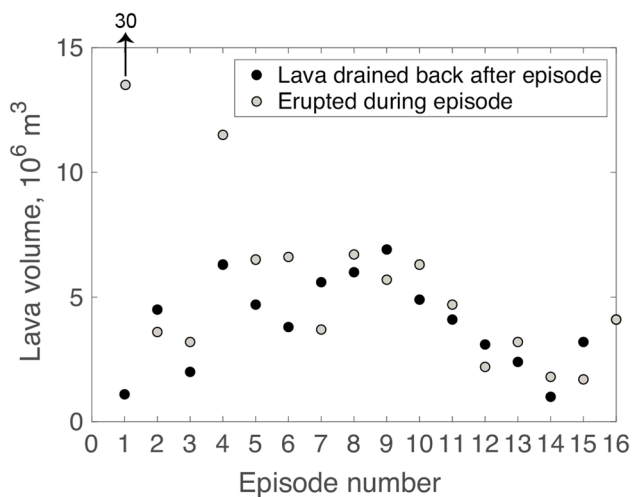
Fig. 2 Volumes of lava erupted and drained back for each episode, calculated using observations of lava lake height combined with tilt data (Eaton et al. 1987; Richter et al. 1970)

Studies of the products of Kīlauea Iki and their progressive cooling and crystallisation in the lava lake that remained at the end of the eruption (Helz and Thornber 1987) allowed the generation of a widely used olivine-liquid thermometer (Helz and Thornber 1987). Lavas erupted from Kīlauea Iki reached a temperature of 1215 °C, the highest in Kīlauea's history (Helz 1987). Eruption samples contained up to 17–20 wt% (on average) of olivine (Wright 1973). The olivines erupted had forsterite contents of 84–88 mol%, which did not vary in any systematic way through the eruption (Helz 1987, 2022). The olivines are too primitive to be in equilibrium with the matrix glass (Sides et al. 2014a). Matrix glass compositions ranged from 6.35 to 10.16 wt% through the eruption (with most falling between 8 and 9 wt%), with the most magnesian glasses produced during episode 1 (Helz 2022). The compositions of the erupted lavas were proposed to be the result of pre-eruptive mixing of two end-member magmas, S1 and S2, which may have been distinct magma batches, together with variable amounts of olivine (Helz 2022). S1 was proposed to have come directly from the mantle (Helz 1987, 2022), perhaps linked to the August 1959 earthquake swarm (Eaton 1962), and may have continued to be intruded into the system up to ~ episode 9 (Helz 1987, 2022). The S2 component was inferred to be more evolved, stored magma (Helz 1987, 2022).

Melt inclusions hosted by olivine have been analysed for volatiles (Anderson and Brown 1993; Sides et al. 2014a; Wallace and Anderson 1998) and trace elements (Sides et al. 2014a). Trace element ratios in the olivine-hosted melt inclusions vary to a much larger degree than in the matrix glasses, consistent either with the mixing of heterogeneous melts coming from the mantle (Sides et al. 2014a) or with

the harvesting of a diverse olivine population (of varying 'ages' and geochemistries) from a sub-caldera mush (Wieser et al. 2019). The water concentrations of melt inclusions decrease systematically through the eruption, from ~ 0.6 wt% for episode 1 to 0.1 to 0.4 wt% for episodes 15 and 16 (Sides et al. 2014a; Wallace and Anderson 1998). The decrease in meltwater contents has been proposed to be due to the mixing of drained back, outgassed melt from the lava lake with primitive, undegassed melt (Sides et al. 2014a; Wallace and Anderson 1998). The water contents of the mixed melts are consistent with the magma budget proposed by Eaton et al. (1987).

Here we examine thin sections of scoria from the longest or most intense episodes, 1, 3, 15 and 16, in order to understand the physical mechanisms of mingling between drained-back lava and undegassed magma in the conduit. We describe and quantify textural evidence for mingling in the erupted products, using optical and scanning electron microscope imagery, combined with image analysis techniques. We present geochemical data for the glass component of erupted pyroclasts for a range of textural types. We evaluate whether there is a change in the textural characteristics of the erupted products due to drain-back and mingling over time through the eruption and whether there are differences in the vesicle population in the recycled component relative to undegassed magma. We develop a simple thermal model that allows us to constrain the origin of the tachylite, and models to describe the reheating and mingling processes responsible for its final form in erupted scoria.

Samples and methods

Sampling and microanalysis

Samples were collected from tephra pits downwind from the scoria cone of Kīlauea Iki. Samples of juvenile lapilli and small bombs were collected from pits KI-07–14, KI-06–16 and KI-06–13 (documented by Stovall et al. 2011, 2012). A complete listing of sample names can be found in the supplementary material. Material was selected from the middle to upper portions of each episode bed. An image of the tephra pit KI-06–13 is shown in Fig. 3, along with a description of the tephra stratigraphy and clast types. The deposits varied significantly in character: episode 1 tephra is dominated by black, glassy achneliths (Walker and Croasdale 1971), including Pele's tears, small glass spheres, shards and rods and fluidal clasts with shiny external surfaces which show flow lines and vesicular interiors with mm- to cm-sized vesicles. Deposits produced by the highest fountains (3, 15 and 16) are characterised by a coarser average grain size of several cm, with dense spatter

Fig. 3 Tephra pit KI-06–13 from which samples were acquired, at Kīlauea Iki scoria cone. Samples from episodes 3, 15 and 16 were obtained from the labelled units. The weaker episodes 5 to 14 have not been clearly separated in this section and appear as a condensed unit. The section is dominated by deposits from high-fountaining episodes (3, 15 and 16), which is reflected in both the thickness of the subunits and dominance of both highly vesicular pumice and large bombs

bombs up to 25 cm in length and ragged, highly vesicular, golden to light brown pumice. Episodes of intermediate height produced tephra with varying proportions of pumice, fluidal clasts and achneliths. Detailed textural and density analyses of clasts from episodes 1, 15 and 16 are presented by Stovall et al. (2011, 2012).

Samples were field-sieved to select at least 100 clasts in the 16–32 mm size fraction (Houghton and Wilson 1989), which were dried in an oven at 122 °C for 24 h to remove water. Polished thin sections were made of a representative set of clasts. The thin sections were scanned optically using a flatbed scanner (CANON CanoScan LiDE 300 Flatbed Scanner) at a resolution of 3200 d.p.i. A Quanta 650F SEM at the University of Cambridge, with a high vacuum and 10 keV accelerating voltage, was used to acquire backscattered electron images of portions of interest of the thin sections, at pixel sizes ranging from 0.01 to 12 μm. Glass compositions were measured using a Cameca SX100 electron probe microanalyser at the University of Cambridge, using a defocused 10 μm beam and an accelerating voltage of 15 kV and beam current 20 nA. Repeated analysis of internal glass standards was used to estimate precision and accuracy for major elements, which are in general better than 5%.

Image processing and vesicle size distributions

Optical scans and SEM images were processed using ImageJ (Abràmoff et al. 2004). The scans were converted to 8-bit images and cropped to remove the edges of each clast. The images all contain varying degrees and forms of a dark-coloured basalt, with high crystallinity, hereafter termed 'tachylite' enclosed in crystal-poor brown glass. The thresholding tool in ImageJ was used to isolate the tachylite component and to calculate its area fraction in the image. Vesicles were highlighted using the thresholding tool. There was some overlap between the greyscale of the vesicles and that of the olivines. A third thresholded image for olivines was generated by adjusting the upper threshold, which allowed for elimination of the olivines in the area fraction calculation of the vesicularity by subtracting one from the other. There remained a small region of greyscale overlap for which it was difficult to correct for we estimate that this could account for up to 5% error on the calculated bulk vesicularities. The 'analyse particles' tool was used to calculate the pixel area and the circularity of each vesicle, as well as other information such as the perimeter length, and the minor and major axes lengths.

These data were used to generate effective radii for each vesicle, then vesicle diameters, using the scaling factor derived from the pixel size in each image. Vesicle sizes were binned using a geometric size factor of $10^{0.1}$ (Sahagian and Proussevitch 1998). A bulk vesicle number density (vesicles per unit area of the image, in mm^{-2}) was calculated for each image and for each size class. In some cases, images were further subcropped to isolate tachylite-dominated regions, to obtain vesicle number densities to compare to those from regions with no tachylite. For pure tachylite and sideromelane 'end member' textures, a sequence of nested SEM images was obtained to combine with the optical scan data in order to produce plots of vesicle number density across a range of size bins. In these cases, two nested SEM images, of 12 and 7 μm resolution, were analysed in the same way as described above, in ImageJ. Vesicle number density plots are generated by combining the three hierarchies of data: the optical scan number densities are used for vesicle size bins > 0.5 mm; and data from two nested SEM images (with pixel sizes of 12 and 7 μm) for bin sizes 0.25–0.4 mm and < 0.25 mm, respectively, after Stovall et al. (2011).

Results

Mingling textures in tephra clasts

A representative selection of optical scans of thin sections showing the mingling textures observed in the tephra clasts from the 1959 Kīlauea Iki eruption is shown in Fig. 4. The tachylite component is dark in colour and contrasts with the lighter brown sideromelane. There is a significant change in the form of the mingled tachylite with time through the eruption. In pyroclasts erupted during episodes 1 and 3, tachylite tends to form discrete inclusions, often taking up most of the volume of the clast. In most clasts, the tachylite inclusions have sharp margins. Scans of samples erupted during episodes 15 and 16 show rather different textural features. In these samples, drawn-out streaks and filaments of tachylite are more common, although discrete inclusions do occur (see Fig. 4m, o). There is evidence of multiple forms (filaments and inclusions) in the same section.
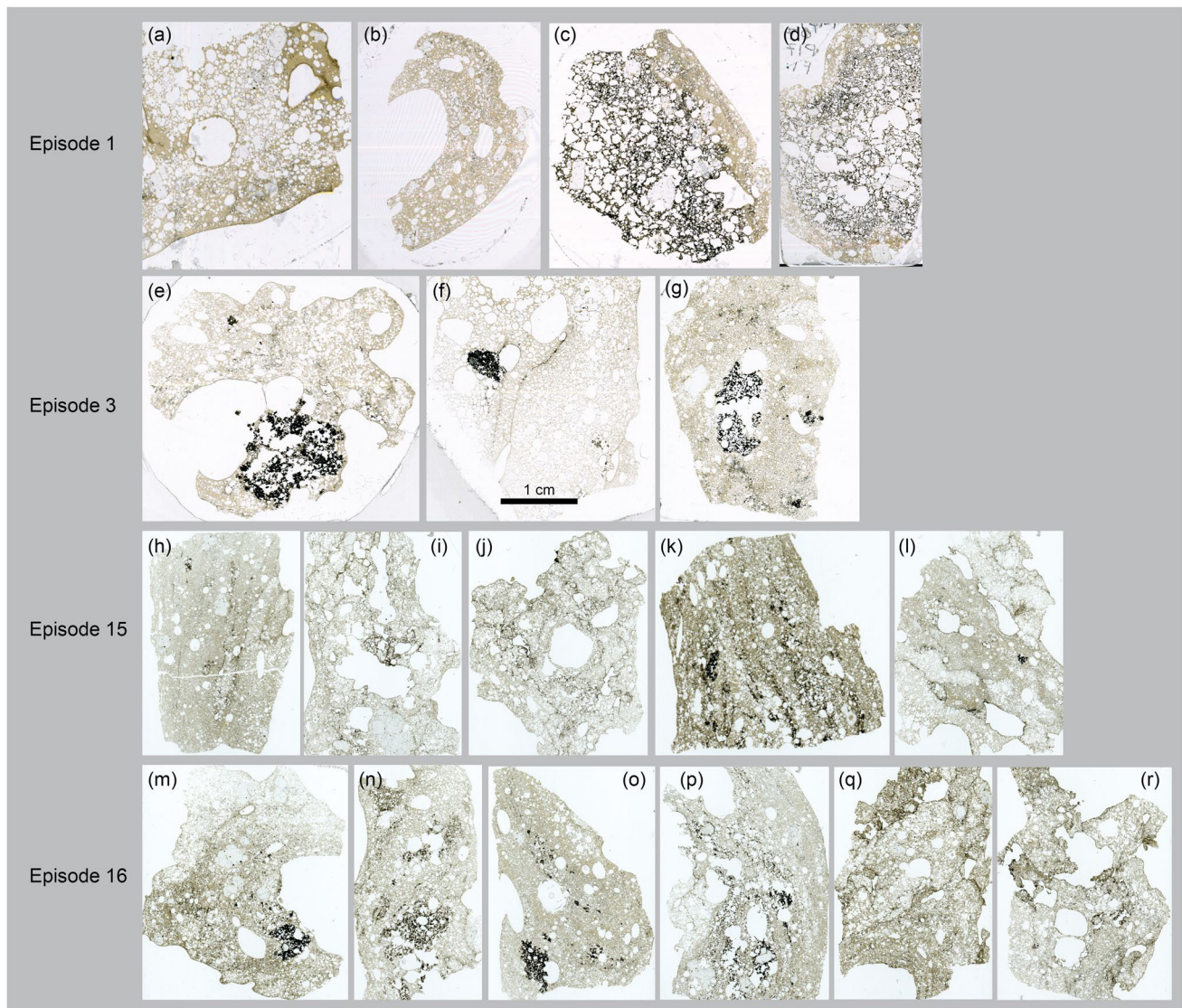

Fig. 4 Optical scans of thin sections of samples erupted during episodes 1, 3, 15 and 16 of the 1959 Kīlauea Iki, showing mingled tachylite components (dark in colour). Episode 1, samples are (from left to right) KI-07–07-ρ20-T10, KI07-07-ρ02-F7, KI07-07-ρ11-F16, KI07-07-ρ17-F1; Episode 3, KI06-13–14-F14, KI06-13–14-T24, KI06-13–14-T17; Episode 15, KI06-13-ρ07, KI06-13-ρ07-T1, KI06-13-ρ07-T5, KI06-13-ρ09-T42, KI06-13-ρ09-T58; Episode 16, KI06-13-ρ01-T19, KI06-13-ρ03-T8, KI06-13-ρ03-T59, KI06-13-ρ05-T4, KI06-13-ρ05-T14, KI06-13-ρ09-T9

Fig. 5 Scanning electron microscope images of crystal types and morphologies in the tachylite component. **a**, **b** KI07-07-ρ20-F1 (episode 1). **c** KI06-13–14-T24 (episode 3). **d** KI06-13-ρ03-T59 (episode 16)
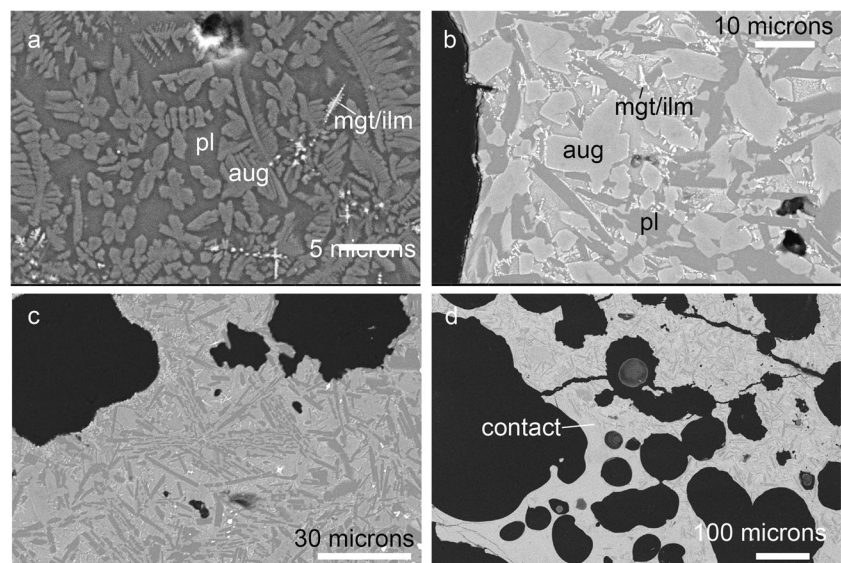
Crystal and glass composition and morphology

The sideromelane component is characterised by clear brown glass, rounded vesicles and the presence of one crystal phase–olivine phenocrysts up to 5 mm in size. The tachylite component is finely crystalline, overall dark in colour, with small microlites of plagioclase, augite and magnetite/ilmenite in the groundmass (Fig. 5). Crystal morphologies include high-aspect ratio rods and swallow-tail crystals of plagioclase and dendritic augite and magnetite/ilmenite (Fig. 5), with magnetite commonly nucleating on the ends of augite crystals.

Single spot electron probe analyses of both types of groundmass glass are shown in Fig. 6 for three representative samples from episode 3 (data may be found in the supplementary material). Also shown are matrix glasses from Helz (2022) for episodes 1, 3, 15 and 16. Sideromelane glass contains ~ 6.9 to 7.5 wt% MgO, consistent with previous studies (Helz 1987, 2022; Sides et al. 2014a). Analyses

of glass from variably crystalline tachylite extend to lower MgO (down to 2.92 wt%), higher K_2O and lower CaO and CaO/Al_2O_3 than the sideromelane component.

Vesicle populations in the sideromelane and tachylite components

Vesicle populations in the tachylite are clearly distinct from those in the sideromelane component (Fig. 7). Vesicles in the sideromelane portions show a greater density of small vesicles (Figs. 7, 8a), and they are rounder. Vesicles in the tachylite are more uniform in size, containing fewer small vesicles, and are more irregular in shape, often with convolute or ragged edges, caused by the vesicles being bounded by interlocked crystal edges (Fig. 8b–d).

Vesicle number densities were measured (vesicles per unit area, N_A, mm^{-2}) in the scans and nested SEM images, and the data were combined (as described in the 'Samples
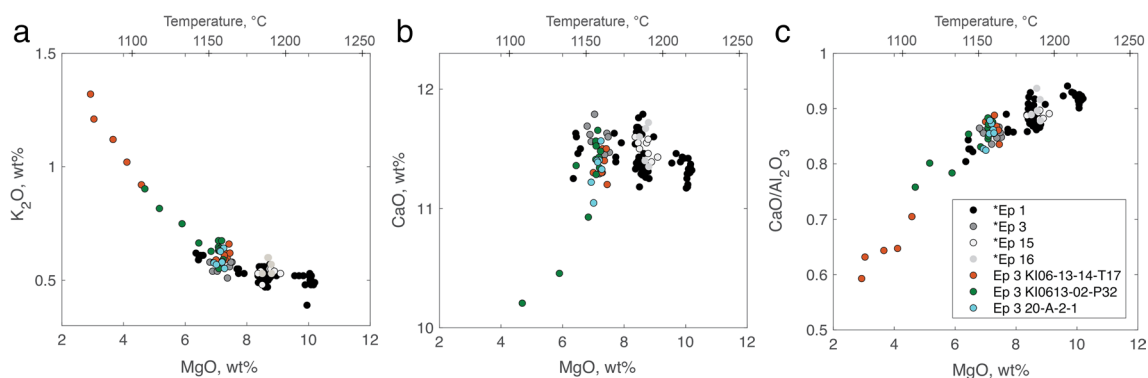

Fig. 6 Electron microprobe data for glasses in three episode 3 samples: KI06-13–14-T17, KI06-13–02-P32, and 20-A-2–1. Plots show MgO (wt%) versus K_2O (wt%) (**a**); CaO (wt%) (**b**); and CaO/Al_2O_3 (**c**), showing a tight cluster of sideromelane glasses at ~ 7.2 +/− 0.4

wt% MgO, with a spread of glasses in the tachylite extending to lower MgO contents. Data may be found in the supplementary material. Also shown, marked with the asterisk '*' in the legend, are episodes 1, 3, 15, and 16 matrix glasses published by Helz (2022)
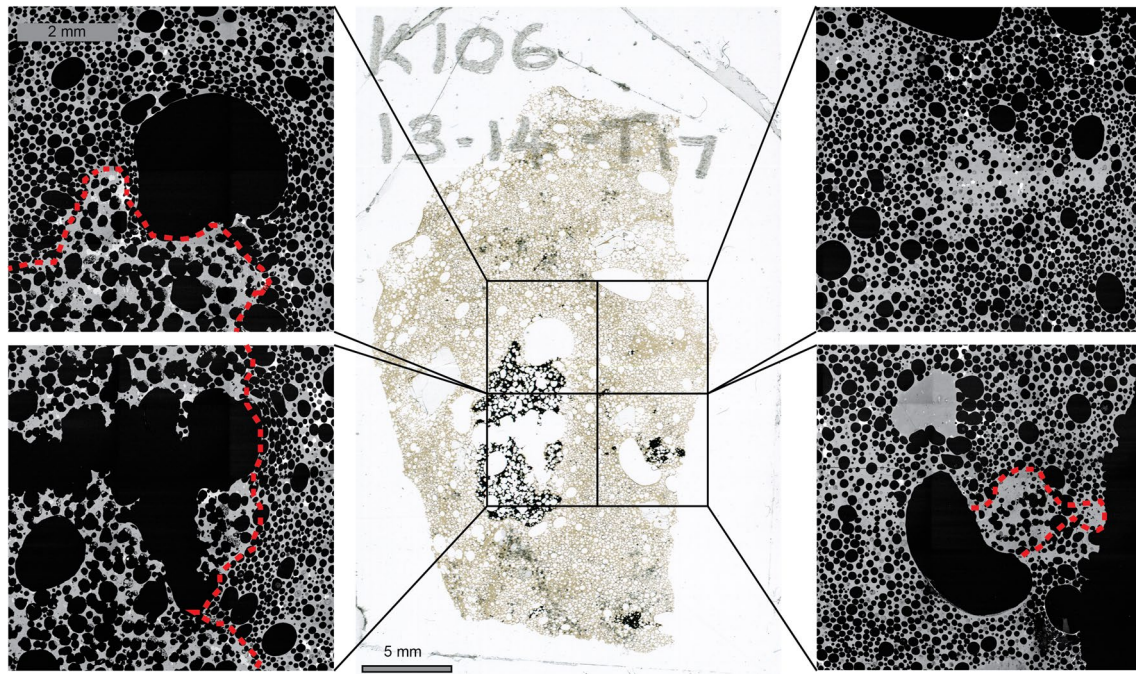
Fig. 7 Scanning electron microscope (SEM) images of portions of the thin section KI06-13–14-T17, erupted during episode 3. The tachylite portion is outlined in red dashed lines in the SEM images. The SEM images are located within the thin section using the opti-cal scan (with black squares showing the location of the SEM image), shown in the middle. In the SEM images, vesicles appear black and groundmass (glass and crystals) grey. Scale for surrounding image are marked on the top left image

Fig. 8 Scanning electron microscope images of vesicle textures in erupted clasts containing tachylite. **a** An olivine phenocryst in pristine sideromelane glass from sample KI06-13-ρ01-T19 (episode 16). **b–d** Vesicle textures in the tachylite component of sample KI06-13-ρ03-T59 (episode 16). **c** Image shows how vesicle texture changes sharply across a tachylite-sideromelane contact
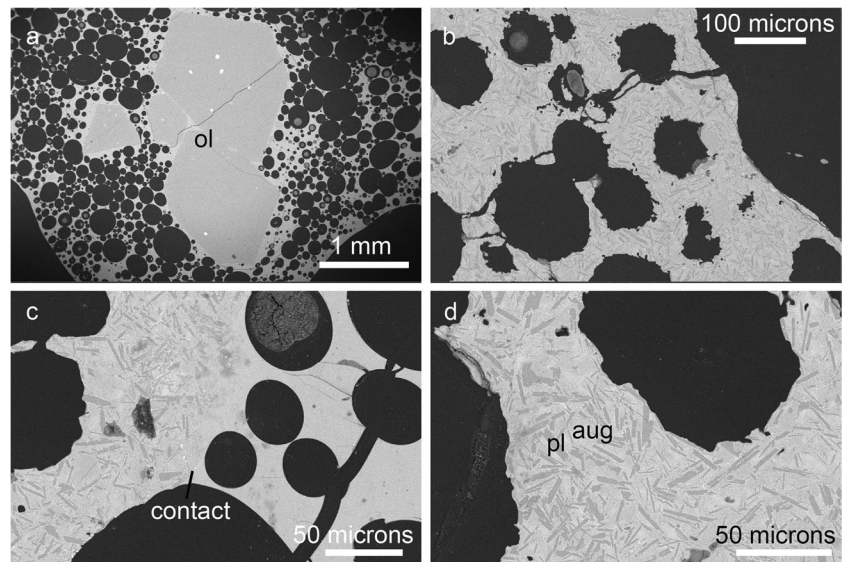
and methods' section) and shown in Fig. 9 and in the supplementary material. The sideromelane vesicle number densities reach their highest values (2–30 mm^{-2}) for vesicle sizes 0.1–0.2 mm. The tachylite data are noisier, owing to the lower number of vesicles in the tachylite clasts and the smaller area fractions available for analysis. However, it is apparent that the tachylite component lacks the large number densities of small bubbles < 0.65 mm and has a higher number densities of larger vesicles > 1 mm, which may indicate a higher degree of bubble coalescence. These features of the tachylite component vesicle population are also obvious from visual inspection of the scan and SEM images (Figs. 7, 8).
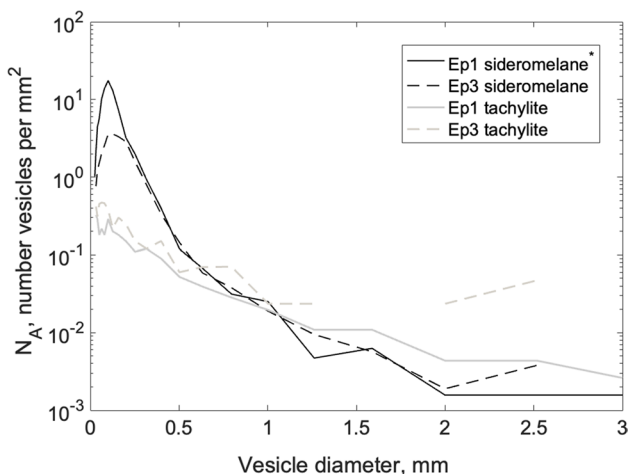
Fig. 9 Vesicles per unit area (N_A) for sideromelane from episode 1 *(Stovall et al. 2011) and episode 3 (sample KI06-13–14-T17) and tachylite from episode 1 (sample KI07-07-ρ11-Tv1) and episode 3 (KI06-13–14-T17). The plots are generated by combining three hierarchies of data: the optical scan number densities are used for vesicle size bins > 0.5 mm; and data from two nested SEM images (with pixel sizes of 12 and 7 μm) for bin sizes 0.25–0.4 mm and < 0.25 mm respectively, after Stovall et al. (2011)

Fig. 10 a A thermal model to predict the thickness of a lava lake crust with base temperatures of 690 and 1070 °C with time, based on the balance between conductive heat loss to the upper layer of the lake and latent heat of crystallisation (Worster et al. 1993) in a crust at the top of the lava lake. In **b** and **c**, we show the frequency distribution of repose times between episodes (x axis as in a), and crust thicknesses calculated using repose times and thermal model, respectively, (y axis as in a)

Discussion

Here we discuss the likely origin of the tachylite component and the nature of the mingling process after drain-back: the formation of a degassed, cool crystallised lava crust on the surface of the lava lake; the initiation of chaotic magma flow in the conduit as a consequence of drain-back of denser degassed lava; and the effect of the chaotic flow on the development of magma mingling textures.

The formation of a lava lake crust

A simple thermal model involving conductive heat loss from the top of the lava lake into the atmosphere (neglecting convection within the interior of the lava lake) allows us to estimate the likely thickness of a crust that might have developed between episodes. We acknowledge this is an over-simplification: it was documented that at times, new lava flowed under the crust remaining from previous episodes, and at other times, it formed a new layer over the old crust (Richter et al. 1970). We assume a fixed and constant initial lava lake temperature, which is well constrained by the mean MgO content in the sideromelane glass, of 1160 °C (Helz and Thornber 1987). As the lateral dimensions of the lake are greater than its depth (1 km versus 125 m) (Richter and Moore 1966), we consider a 1-D model (Fig. 11). As heat is extracted from the upper surface of the lake, a crust that is comprised of glass
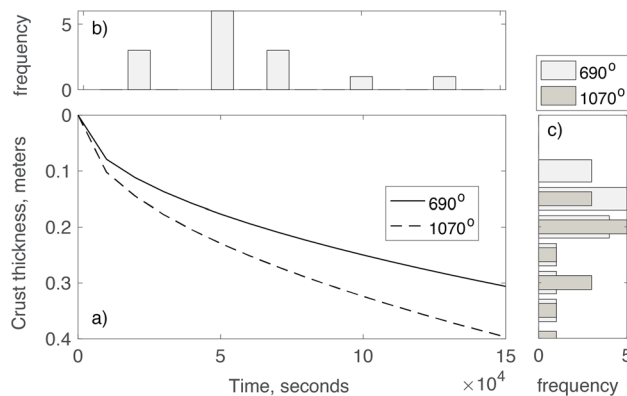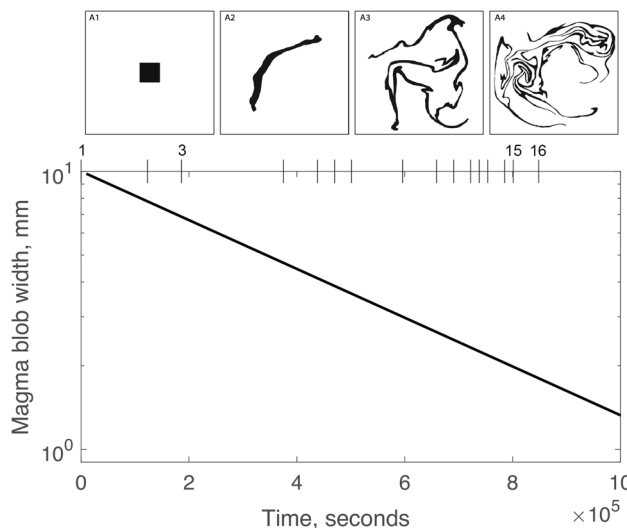

Fig. 11 Top, the process of progressive stretching and folding of magma blobs within another magma host is proposed to produce commonly observed magma mingling textures (sketches at the top from Petrelli et al. 2011). Bottom, the application of a simple dimensionless model to understand how the width of an entrained magma blob may decrease with time during chaotic magma flow shows that, when translated to real dimensions the width of a 10-mm blob can decrease to ~ 1 mm over around $10.^6$ s, or ~ 12 days. The timings of episodes 1–16 are marked on the top of the plot; episodes 1, 3, 15, and 16 are labelled (see text for the detail of the model)

and crystals is formed. In the absence of convection, the thermal balance governing the thickness of the crust is between the transfer of heat by conduction to the upper

boundary and the loss of latent heat of crystallisation (Worster et al. 1993):

$$h \sim \left(\frac{(T_g - T_a)C_p \kappa}{L} \right)^{1/2} t^{1/2} \qquad (1)$$

where h is the thickness of the crust in metres, T_g is the temperature at the base of the crust (°C), T_a is the temperature of the air (°C), C_p is the specific heat of basalt ($Jkg^{-1} K^{-1}$), κ is the thermal diffusivity (m^2/s), L is the latent heat (Jkg^{-1}) and t is the time in seconds.

We use a range of temperatures for the base of the crust: 690 °C is the glass transition temperature for Kīlauea basalt (Giordano et al. 2005); and 1070 °C corresponds to a lock-up crystallinity of ~50 vol% (estimated by noting from Fig. 6 that the K_2O content of the episode 3 sideromelane is 0.6 wt% and increases to 1.2 wt% on cooling to ~1070 °C, i.e. after ~50% of the liquid crystallised). These two temperatures give a range of length scales: for a thin glassy crust and an extensively crystallised rigid lava lid (Fig. 10). Our model yields crust thicknesses of 10 to 40 cm for the cooling periods defined by the typical intervals between episodes (4–52 h; Richter et al. 1970). We note that this thickness represents a minimum thickness for a partially crystalline, brittle glassy layer. We note that cooling times may have been much shorter (and crust thicknesses much less), as the lake was filling throughout the episode and perhaps resurfacing during that time (Richter et al. 1970; Stovall et al. 2009a, 2009b).

The crust thickness of 8–35 cm and the maximum depth of the lake during and between episodes of 125 m (Eaton et al 1987) yield a volume proportion of 0.06 to 0.28 vol% of cooler brittle crust compared to the sub-crustal hot basalt that drained back into the conduit during and after the end of each episode. We have not carried out a systematic analysis of tachylite volume proportions and clast size on hand specimen scales, but qualitative observations of randomly generated thin sections suggest that the volume proportion of tachylite in the erupted scoria is low (<<1%). Our simple analysis serves to demonstrate that lava lake crust fragments of a size like the re-erupted tachylite clasts may have been formed by quenching at the lava lake surface during the intervals between fountaining episodes and that the observed volume fraction of these fragments is approximately consistent with a cooled lava lake crust origin.

Overturn of the lava lake crust occurred repeatedly throughout the eruption, taking place both during the filling and draining of the lake (Richter et al. 1970). Localised events often led to 'wholescale foundering' of the crust (Richter et al. 1970). A foundering event preserved in place near the end of the eruption allowed these mechanisms to be constrained in more detail (Stovall et al. 2009b): the crust may have destabilised when the lava beneath drained away, then become overrun by fresh advancing lava of a lower density, causing the relatively dense, gas-poor solid crust to sink (Stovall et al. 2019b).

Textural modification of recycled clasts during reheating

The dimensions of the recycled fragments of lava lake crust are in the range 0.01–1 m (from observation at outcrop scale) which, when considered alongside the value for thermal diffusivity for basalt (1×10^{-6} m^2/s), yields approximate timescales of thermal homogenisation in the conduit on the order of 0.4 min for 1 cm fragments to 42 min for 10 cm fragments to 69 h for metre-scale fragments, i.e. similar to the repose times between eruption episodes (4–52 h; Fig. 10). This analysis suggests that recycled clasts will undergo significant heating above their glass transition temperature, which may induce devitrification and further crystallisation (Burkhard 2001; Deardorff and Cashman 2017), and overprint any crystallisation textures formed during quench cooling in the lava lake crust.

The textural and petrological features of the tachylite are consistent with those observed after reheating basaltic sideromelane glass-rich samples in experiments (Burkhard 2001; D'Oriano et al. 2014; D'Oriano et al. 2013; Deardorff and Cashman 2017). Crystallisation in magmas is usually prompted by cooling or degassing, but reheating glassy basalt to temperatures above the glass transition, which is ~690 °C for basalt (Giordano et al. 2005), but below the liquidus temperature, can induce extensive crystallisation (devitrification) and oxidation (Burkhard 2001; D'Oriano et al. 2013; Deardorff and Cashman 2017). The dark colour of the tachylite component is a consequence of the high proportion of microlites of magnetite and augite present (Fig. 5) (Deardorff and Cashman (2017) observed the appearance of diffusion-controlled dendritic pyroxene and oxides at temperatures > 690 °C) in heating experiments on natural samples of quenched, glassy sideromelane from Parícutin (Mexico), starting at room temperature and atmospheric pressure. Plagioclase appears at temperatures of 900 °C, with elongate lath morphologies (Deardorff and Cashman 2017), similar to those we observe in the Kīlauea samples (Fig. 5). Reheating experiments carried out on glassy Kilauea basalt samples in air showed that at below 840 °C, pyroxene dendrites grew with Fe-Ti oxides at their apices (Burkhard 2001), remarkably similar in texture to the tachylite in this study (Fig. 5). In the experiments, there is initially an increase in crystallinity, as the temperature is raised above the glass transition, then a decrease as the temperature approaches (to within 30 °C) the liquidus for Parícutin basalt samples (Deardorff and Cashman 2017). We propose that the ragged edges to vesicles observed in the tachylite (Fig. 8) are evidence that crystal growth occurred post-vesiculation in these clasts, with originally smooth and rounded vesicle walls becoming

disrupted by crystal growth in an increasingly ductile melt. As the temperature was increased to temperatures > 1100 °C in the experiments, the glass began to flow, forming streaks. In our samples, streaks and filaments are more common in the products of the later episodes of the eruption, suggesting that these clasts have been held and heated in the hot magma for longer, perhaps over multiple eruption drain-back cycles.

Magma mingling during chaotic flow in the conduit

Drain-back of degassed lava may be expected to induce convection in the conduit, with the denser, degassed component sinking relative to the hotter, more gas-rich component. Convection may lead to chaotic flow, which may promote mingling, i.e. stretching and folding (Morgavi et al. 2022; Oldenburg et al. 1989; Petrelli et al. 2011). Magma convection driven by density differences caused by degassing has been invoked to be taking place beneath lava lakes over a length-scale of ~ 1 km at Kīlauea Volcano summit during 2008–2023, based on observations of glass geochemistry, lake level, gas fluxes and gravity anomalies (Carbone and Poland 2012; Edmonds et al. 2013; Patrick et al. 2015, 2016).

The density difference between drained-back and conduit magma would be controlled principally by the differences in the exsolved gas content, which will influence bulk magma density to a large degree and to a lesser degree by differences in dissolved water (Wallace and Anderson 1998; Sides et al. 2014a). Using the partial molar volume for dissolved water of 22.9606 cm^3/mol at 1000 °C and 1 bar of pressure (Ochs and Lange 1999), we calculate a density difference of 20 kg/m^3 based on loss of 1 wt% water on eruption. Stovall et al. (2009a) studied the differences in density between a lava lake crust and underlying 'squeeze up' pahoehoe at the Kīlauea Iki lava lake and found a bulk density difference of 737 kg/m^3, due to the contrasting vesicularities caused by variable degrees of outgassing from the lava lake surface.

We can calculate the Rayleigh number (Ra) for the system of dense degassed magma draining back into hot vesiculating magma in the conduit to assess whether there is a sufficient density heterogeneity to set up a chaotic flow, which has potential to mingle the two magmas and deform clasts of lava crust. Ra is given by:

$$Ra = \frac{\Delta \rho l^3 g}{\eta \alpha} \tag{2}$$

where l is the length scale of mingling (we use 5–10 m as an estimate of conduit diameter), $\Delta \rho$ is the density difference between water-bearing basalt and degassed basalt (estimated to be 20–737 kg/m^3), g is acceleration due to gravity, η is viscosity of the water-bearing hot basalt (10–100 Pas) and α is the thermal diffusivity (1×10^{-6} m^2/s). We estimate Ra to

lie in the range 10^9 to 10^{10}, which would be consistent with chaotic magma flow due to the density contrasts.

A range of numerical models have been developed to understand the onset of chaotic mingling and mixing in magma reservoirs (Petrelli et al. 2011; others). It has been proposed that mingling textures develop through repeated stretching and folding that take place at high Rayleigh numbers (> 10^7; Oldenburg et al. 1989; Petrelli et al. 2011). The timescale for the stretching of mingled magma enclaves or parcels of magma enclosed in a second magma host is primarily governed by a characteristic rate of stretching of a blob of magma, which has been shown to be remarkably constant in dimensionless terms over a range of buoyancy and viscosity contrasts between the two magmas (Petrelli et al. 2011), with the form:

$$d' = d'_0 e^{(-at')} \tag{3}$$

where d_0' is the dimensionless width of an initial magma blob inside a different host magma, equal to the ratio between the size of the blob and the dimension of the host magma 'cell' enclosing it, approximated as 0.001 for this system (equivalent to a 1 cm recycled lava blob inside a 10 m dimension volume of host magma). The term λ is a constant equal to the rate of decrease in filament width per unit of dimensionless time, here taken as 0.02 (from Petrelli et al. 2011) multiplied by a constant a (equal to 10^4). Dimensionless time, t', is given by the ratio $\kappa/{d^2}$, where κ is the thermal diffusivity (m^2/s) and d is the dimension of the magma host 'cell'. This model shows that filament thickness for these length scales is predicted to decrease from 10 to 8 mm in 30 h and to 1 mm over approximately 12 days (Fig. 11). The timings of the 16 episodes of the eruption are marked in Fig. 11. This analysis suggests that if recycled clasts are re-erupted rapidly then they will undergo only minor stretching and folding, if they are drained back and re-erupted over many episodes, then they have the potential to become highly stretched (by a factor of ~ 10) and folded. This analysis may explain why scoria from the later episodes (15 and 16) contain a greater proportion of tachylite filaments and streaks relative to episodes 1 and 3 (Fig. 4). We note that as well as chaotic flow due to buoyancy contrasts, there will also be lateral flow of the magma related to eruption, lava lake filling and drain-back, which will contribute to the mingling process.

Conclusions

Glassy basaltic scoria erupted during the 1959 Kīlauea Iki (Hawai'i) eruption contains extensive and pervasive evidence of mingling of the co-erupted magma in the form of inclusions and streaks of tachylite. The tachylite is dark with high crystallinity, comprised of < 10 μm dendrites of plagioclase, augite and magnetite–ilmenite. The vesicle population

of the tachylite is distinct from the host glassy basalt: it is missing the smallest vesicle size fraction and has overall fewer and larger and more irregularly-shaped vesicles, with evidence of micron-scale, local, ductile deformation on the vesicle walls. Mingling textures became more complex through the eruption, with tephra from episodes 15 and 16 showing complex mingling, with more abundant streaks and filaments of the tachylite component.

We infer that the tachylite component in this case represents recycled lava derived from the chilled skin of the lava lake, which was transported back into the conduit during drain-back at the end of each episode. We construct thermal models to establish that a lava lake crust could develop on the timescale of episode repose times and that crust fragments of these dimensions would undergo partial or complete thermal homogenisation in the conduit over hours to days. Heating of the recycled fragments would have triggered devitrification and crystallisation of dendrites. Due to the density difference between drained back and conduit magma, convective chaotic flow would have developed in the conduit, providing a means to stretch and fold these recycled, reheated crust fragments. We propose that some of these fragments may have been erupted and drained back during multiple episode cycles, resulting in a higher proportion of thin tachylite filaments being observed in products of the later episodes.

Data availability All data is included in the Supplementary Information.

Declarations

Competing interests The authors declare no competing interests.

References

Abràmoff MD, Magalhães PJ, Ram SJ (2004) Image processing with ImageJ. Biophoton Int 11(7):36–42

Anderson AT, Brown GG (1993) CO2 contents and formation pressures of some Kilauean melt inclusions. Am Mineral 78(7–8):794–803

Andrews BJ, Manga M (2014) Thermal and rheological controls on the formation of mafic enclaves or banded pumice. Contrib Mineral Petrol 167(1):961

Andronico D, Cristaldi A, Del Carlo P, Taddeucci J (2009) Shifting styles of basaltic explosive activity during the 2002–03 eruption of Mt Etna, Italy. J Volcanol Geotherm Res 180(2–4):110–122

Bateman R (1995) The interplay between crystallization, replenishment and hybridization in large felsic magma chambers. Earth-Sci Rev 39(1–2):91–106

Burkhard DJ (2001) Crystallization and oxidation of Kilauea basalt glass: processes during reheating experiments. J Petrol 42(3):507–527

Carbone D, Poland MP (2012) Gravity fluctuations induced by magma convection at Kīlauea Volcano, Hawai'i. Geology 40(9):803–806

Cimarelli C, Di Traglia F, Taddeucci J (2010) Basaltic scoria textures from a zoned conduit as precursors to violent Strombolian activity. Geology 38(5):439–442

D'Oriano C, Cioni R, Bertagnini A, Andronico D, Cole P (2011) Dynamics of ash-dominated eruptions at Vesuvius: the post-512 AD AS1a event. Bull Volcanol 73(6):699–715

D'Oriano C, Pompilio M, Bertagnini A, Cioni R, Pichavant M (2013) Effects of experimental reheating of natural basaltic ash at different temperatures and redox conditions. Contrib Miner Petrol 165(5):863–883

D'Oriano C, Bertagnini A, Cioni R, Pompilio M (2014) Identifying recycled ash in basaltic eruptions. Sci Rep 4(1):5851

Deardorff N, Cashman K (2017) Rapid crystallization during recycling of basaltic andesite tephra: timescales determined by reheating experiments. Sci Rep 7:46364

Eaton J, Richter D, Krivoy H (1987) Cycling of magma between the summit reservoir and Kīlauea Iki lava lake during the 1959 eruption of Kīlauea volcano: US Geol. Surv Prof Pap 1350:1307–1335

Eaton JP (1962) Crustal structure and volcanism in Hawaii. In: Smith WE, Macdonald GA, Kuno H (eds) The Crust of the Pacific Basin. https://doi.org/10.1029/GM006p0013

Edmonds M, Sides I, Swanson D, Werner C, Martin R, Mather T, Herd R, Jones R, Mead M, Sawyer G (2013) Magma storage, transport and degassing during the 2008–10 summit eruption at Kilauea Volcano Hawaii. Geochimica Cosmochim Acta 213:284–301

Giordano D, Nichols AR, Dingwell DB (2005) Glass transition temperatures of natural hydrous melts: a relationship with shear viscosity and implications for the welding process. J Volcanol Geoth Res 142(1–2):105–118

Heiken G (1978) Characteristics of tephra from cinder cone, Lassen volcanic national park, California. Bull Volcanol 41(2):119–130

Helz RT (1987) Diverse olivine types in lava of the 1959 eruption of Kilauea volcano and their bearing on eruption dynamics. US Geol Surv Prof Pap 1350:691–722

Helz RT (2022) Proportions, timing, and re-equilibration progress during the 1959 summit eruption of Kīlauea: an example of magma mixing processes operating during OIB petrogenesis. J Petrol 63(1):egab091

Helz RT, Thornber CR (1987) Geothermometry of Kilauea Iki lava lake Hawaii. Bull Volcanol 49(5):651–668

Houghton B, Wilson C (1989) A Vesicularity Index for Pyroclastic Deposits. Bull Volcanol 51(6):451–462

Jarvis PA, Pistone M, Secretan A, Blundy JD, Cashman KV, Mader HM, Baumgartner LP (2021) Crystal and volatile controls on the

mixing and mingling of magmas: Crustal Magmatic System Evolution: Anatomy, Architecture, and Physico-Chemical Processes, pp 125–150

Kremers S, Lavallée Y, Hanson J, Hess KU, Chevrel MO, Wassermann J, Dingwell DB (2012) Shallow magma-mingling-driven Strombolian eruptions at Mt. Yasur volcano, Vanuatu. Geophys Res Lett 39(21). https://doi.org/10.1029/2012GL053312

Lautze NC, Houghton BF (2005) Physical mingling of magma and complex eruption dynamics in the shallow conduit at Stromboli volcano Italy. Geology 33(5):425–428

Lautze NC, Houghton BF (2007) Linking variable explosion style and magma textures during 2002 at Stromboli volcano Italy. Bull Volcanol 69(4):445–460

Lynn KJ, Garcia MO, Shea T, Costa F, Swanson DA (2017) Timescales of mixing and storage for Keanakāko 'i Tephra magmas (1500–1820 CE), Kīlauea Volcano, Hawai 'i. Contrib Mineral Petrol 172(9):76

Morgavi D, Laumonier M, Petrelli M, Dingwell DB (2022) Decrypting magma mixing in igneous systems. Rev Mineral Geochem 87(1):607–638

Murphy MD, Sparks R, Barclay J, Carroll MR, Lejeune A-M, Brewer TS, MacDonald R, Black S (1998) The role of magma mixing in triggering the current eruption at the Soufriere Hills Volcano, Montserrat. Geophys Res Lett 25:3433–3436

Neave DA, Passmore E, Maclennan J, Fitton G, Thordarson T (2013) Crystal–melt relationships and the record of deep mixing and crystallization in the ad 1783 Laki Eruption. Iceland. J Petrol 54(8):1661–1690

Ochs FA III, Lange RA (1999) The density of hydrous magmatic liquids. Science 283(5406):1314

Oldenburg CM, Spera FJ, Yuen DA, Sewell G (1989) Dynamic mixing in magma bodies: theory, simulations, and implications. J Geophys Res Solid Earth 94(B7):9215–9236

Owen J, Shea T, Tuffen H (2019) Basalt, unveiling fluid-filled fractures, inducing sediment intra-void transport, ephemerally: examples from Katla 1918. J Volcanol Geoth Res 369:121–144

Patrick MR, Anderson KR, Poland MP, Orr TR, Swanson DA (2015) Lava lake level as a gauge of magma reservoir pressure and eruptive hazard. Geology 43(9):831–834

Patrick MR, Orr T, Swanson D, Lev E (2016) Shallow and deep controls on lava lake surface motion at Kīlauea Volcano. J Volcanol Geotherm Res 328:247–261

Perugini D, Poli G (2012) The mixing of magmas in plutonic and volcanic environments: analogies and differences. Lithos 153:261–277

Perugini D, Poli G, Gatta G (2002) Analysis and simulation of magma mixing processes in 3D. Lithos 65(3–4):313–330

Perugini D, Poli G, Mazzuoli R (2003) Chaotic advection, fractals and diffusion during mixing of magmas: evidence from lava flows. J Volcanol Geotherm Res 124(3–4):255–279

Petrelli M, Perugini D, Poli G (2011) Transition to chaos and implications for time-scales of magma hybridization during mixing processes in magma chambers. Lithos 125(1–2):211–220

Pioli L, Erlund E, Johnson E, Cashman K, Wallace P, Rosi M, Granados HD (2008) Explosive dynamics of violent Strombolian eruptions: the eruption of Parícutin Volcano 1943–1952 (Mexico). Earth Planet Sci Lett 271(1–4):359–368

Plail M, Edmonds M, Woods AW, Barclay J, Humphreys MC, Herd RA, Christopher T (2018) Mafic enclaves record syn-eruptive basalt intrusion and mixing. Earth Planet Sci Lett 484:30–40

Pompilio M, Bertagnini A, Carlo P, Roberto A (2017) Magma dynamics within a basaltic conduit revealed by textural and compositional features of erupted ash: the December 2015 Mt. Etna Paroxysms. Sci Rep 7(1):4805

Richter DH, Moore JG (1966) Petrology of the Kilauea Iki lava lake, Hawaii: U.S. Geological Survey Professional Paper 537-B, p 26. https://doi.org/10.3133/pp537B

Richter DH, Eaton J, Murata K, Ault W, Krivoy H (1970) Chronological narrative of the 1959–60 eruption of Kīlauea Volcano, Hawaii. In: The 1959–60 eruption of K lauea volcano, Hawai'i. US Geol Sury Prof Pap, 537-E:E1–E73

Ruprecht P, Bergantz GW, Dufek J (2008) Modeling of gas-driven magmatic overturn: tracking of phenocryst dispersal and gathering during magma mixing. Geochem Geophys Geosyst 9(7). https://doi.org/10.1029/2008GC002022

Sahagian DL, Proussevitch AA (1998) 3D particle size distributions from 2D observations: stereology for natural applications. J Volcanol Geotherm Res 84(3–4):173–196

Schleicher JM, Bergantz GW, Breidenthal RE, Burgisser A (2016) Time scales of crystal mixing in magma mushes. Geophys Res Lett 43(4):1543–1550

Sides I, Edmonds M, Maclennan J, Houghton B, Swanson D, Steele-MacInnis M (2014a) Magma mixing and high fountaining during the 1959 Kīlauea Iki eruption, Hawai'i. Earth Planet Sci Lett 400:102–112

Sides IR, Edmonds M, Maclennan J, Swanson DA, Houghton BF (2014b) Eruption style at Kīlauea Volcano in Hawai'i linked to primary melt composition. Nat Geosci 7:464–469

Sparks R, Marshall L (1986) Thermal and mechanical constraints on mixing between mafic and silicic magmas. J Volcanol Geoth Res 29(1–4):99–124

Sparks SR, Sigurdsson H, Wilson L (1977) Magma mixing: a mechanism for triggering acid explosive eruptions. Nature 267(5609):315–318

Stovall WK (2009) Dynamics and processes during the 1959 Kīlauea Iki eruption, University of Hawaii at Manoa

Stovall W, Houghton BF, Harris AJ, Swanson DA (2009a) Features of lava lake filling and draining and their implications for eruption dynamics. Bull Volcanol 71:767–780

Stovall WK, Houghton BF, Harris A, Swanson D (2009b) A frozen record of density-driven crustal overturn in lava lakes: the example of Kīlauea Iki 1959. Bull Volcanol 71:313–318

Stovall W, Houghton BF, Gonnermann H, Fagents SA, Swanson DA (2011) Eruption dynamics of Hawaiian-style fountains: the case study of episode 1 of the Kīlauea Iki 1959 eruption. Bull Volcanol 73(5):511–529

Stovall W, Houghton B, Hammer J, Fagents S, Swanson D (2012) Vesiculation of high fountaining Hawaiian eruptions: episodes 15 and 16 of 1959 Kīlauea Iki. Bull Volcanol 74(2):441–455

Taddeucci J, Pompilio M, Scarlato P (2004) Conduit processes during the July–August 2001 explosive activity of Mt. Etna (Italy): inferences from glass chemistry and crystal size distribution of ash particles. J Volcanol Geotherm Res 137(1–3):33–54

Viccaro M, Ferlito C, Cortesogno L, Cristofolini R, Gaggero L (2006) Magma mixing during the 2001 event at Mount Etna (Italy): effects on the eruptive dynamics. J Volcanol Geotherm Res 149(1):139–159

Walker GPL, Croasdale R (1971) Characteristics of Some Basaltic Pyroclastics. Bull Volcanol 35(2):303–317

Wallace PJ, Anderson AT (1998) Effects of eruption and lava drainback on the H2O contents of basaltic magmas at Kīlauea Volcano. Bull Volcanol 59(5):327–344

Wieser PE, Edmonds M, Maclennan J, Jenner FE, Kunz BE (2019) Crystal Scavenging from Mush Piles Recorded by Melt Inclusions. Nat Commun 10(1):1–11

Woods AW, Cowan A (2009) Magma mixing triggered during volcanic eruptions. Earth Planet Sci Lett 288(1):132–137

Worster MG, Huppert HE, Sparks RSJ (1993) The crystallization of lava lakes: Journal of Geophysical Research: Solid. Earth 98(B9):15891–15901

Wright TL (1973) Magma mixing as illustrated by the 1959 eruption, Kīlauea Volcano, Hawaii. Geol Soc Am Bull 84(3):849–858